https://doi.org/10.5194/gmd-2020-287
Preprint. Discussion started: 9 November 2020

Geoscientific Model Development Discussions

Sensitivity of Northern Hemisphere climate to ice-ocean interface heat flux parameterizations

Xiaoxu Shi[1], Dirk Notz[2,3], Jiping Liu[4], Hu Yang[1], and Gerrit Lohmann[1]

[1]Alfred Wegener Institute, Helmholtz center for Polar and Marine Research, Bremerhaven, Germany
[2]Institute for Oceanography, Center for Earth System Research and Sustainability (CEN), Hamburg University, Hamburg, Germany
[3]Max Planck Institute for Meteorology, Hamburg, Germany
[4]Department of Atmospheric and Environmental Sciences, University at Albany, New York, USA

Correspondence: Xiaoxu Shi (xshi@awi.de)

Abstract. We investigate the impact of three different parameterizations of ice-ocean heat exchange on modeled ice thickness, ice concentration, and water masses. These three parameterizations are (1) an ice-bath assumption with the ocean temperature fixed at the freezing temperature, (2) a turbulent heat-flux parameterization with ice-ocean heat exchange depending linearly on the temperature difference between the mixed layer and the ice-ocean interface, and (3) a similar turbulent heat-flux parameterization as (2) but with the temperature at the ice-ocean interface depending on ice-ablation rate. Based on model simulations with the standalone sea-ice model CICE, the ice-ocean model MPIOM and the climate model COSMOS, we find that (3) leads (in comparison to the other two parameterizations) to a thicker modeled sea ice, warmer water beneath high-concentration ice and cooler water towards the ice edge, and higher salinity in the Arctic Ocean mixed layer. Finally, in the fully coupled climate model COSMOS, the most realistic parameterization leads to an enhanced Atlantic meridional overturning circulation (AMOC), a more positive North Atlantic Oscillation (NAO) mode and a weakened Aleutian Low.

1 Introduction

The growth and decay of sea ice at the ice–ocean interface are determined by the local imbalance between the conductive heat flux within the ice and the oceanic heat flux from below the ice. Because the temperature at the ice–ocean interface is determined by phase equilibrium, any imbalance between the two fluxes is not compensated by changes in the local temperature as is the case at the ice surface, but instead by ice growth or ablation. This makes the evolution of sea ice thickness very sensitive to small changes in oceanic heat flux (e.g. *Maykut and Untersteiner*, 1971). Thus a realistic parameterization of flux exchanges at the ice-ocean interface is important for simulating sea ice and its climate feedback.

For the simplest parameterization, the ice–ocean system is simply treated as an ice bath (c.f. *Schmidt et al.*, 2004): The temperature of the uppermost ocean grid cells is fixed at the freezing temperature, and any excess energy that enters these grid

https://doi.org/10.5194/gmd-2020-287
Preprint. Discussion started: 9 November 2020


Geoscientific Model Development Discussions

cells via advection, convection, or heat exchange with the atmosphere is instantaneously applied to the ice through lateral and bottom melting. Such parameterization is consistent with turbulence models that treat the flux of heat and salt as analogous to momentum flux (*Josberger*, 1983; *Mellor et al.*, 1986), which results in very efficient transfer whenever the ice is in motion relative to the underlying water. However, the ice-bath paradigm is incompatible with observations (i.e., the 1984 Marginal Ice Zone Experiment (MIZEX)), which clearly indicate that an ice-covered mixed layer can store significant amounts of heat (i.e., remain above freezing) for extended periods of time (*McPhee*, 1986; *McPhee et al.*, 1987; *Perovich and Maykut*, 1990). These measurements demonstrate that in particular during melting, the exchange of scalar quantities such as heat and salt differs significantly from the exchange of momentum. The reason for this lies in the fact that, unlike ice-ocean momentum flux, heat and mass transfer are strongly affected by a thin sublayer controlled by molecular processes (*McPhee et al.*, 1987). Consistent with laboratory studies of heat transfer over hydraulically rough surfaces (*Yaglom and Kader*, 1974), the heat exchange is hence not only determined by turbulent processes but also by diffusion through this molecular sublayer.

The fact that the oceanic temperature can be significantly higher than the freezing temperature even underneath a dense ice cover cannot be represented in numerical models that employ an ice-bath assumption. More advanced formulations of ice–ocean heat exchange are therefore based on bulk formula, where the ice–ocean heat exchange depends linearly on the temperature difference between the mixed layer and the ice–ocean interface. Early models used a constant diffusion term as the proportionality constant (*Røed*, 1984), while more advanced formulations made the heat exchange depend on friction velocity as well (*McPhee*, 1992). For such more advanced formulations, measurements show proportionality between heat flux and temperature difference times friction velocity across a large range of Reynolds numbers (e.g., Fig. 6.5 in *McPhee*, 2008). These formulations form the basis of many modern sea-ice models (e.g. *Hunke and Lipscomb*, 2010).

These formulations, despite being physically much more realistic than the crude ice-bath assumption, often suffer from the fact that the temperature at the ice–ocean interface is simply set as the freezing temperature of the underlying sea water. In reality, however, the interfacial temperature is determined by *local* phase equilibrium, and in particular during periods of high ablation rates, the local salinity at the interface can be significantly lower than the salinity of the sea water underneath. The interfacial temperature can be significantly higher than the freezing temperature of the underlying sea water. Therefore, one extension of the turbulent parameterizations of ice–ocean heat exchange lies in the explicit calculation of the temperature at the ice–ocean interface based on local salinity (*Jenkins et al.*, 2001; *Notz et al.*, 2003; *Schmidt et al.*, 2004). Such formulations then allow for the explicit calculation of heat and salt fluxes, and give a more realistic estimate of ice–ocean heat exchange. In particular, these formulations allow for the ice–ocean interface to be warmer than the underlying sea water, which allows for heat fluxes from the interface into the underlying ocean. This becomes in particular important whenever large amounts of meltwater accumulate underneath sea ice during summer (*Notz et al.*, 2003).

In this study, we examine how different physical realism that is represented by the three discussed parameterizations impact the resulting ice cover, large-scale oceanic circulation, and atmosphere properties in numerical models. The paper is organized as follows. Section 2 describes the parameterizations in details. Section 3 introduces various models that we use for our purposes, including a conceptual 1-dimensional model that allows us to examine a wide parameter range, the standalone sea-ice model CICE that allows us to determine changes of sea ice in a modern sea-ice model, the ocean–sea-ice model MPIOM,

https://doi.org/10.5194/gmd-2020-287
Preprint. Discussion started: 9 November 2020


Geoscientific Model Development Discussions
Open Access
EGU

which allows us to examine the impact of the parameterizations on the large-scale ocean circulation, and the fully coupled climate model COSMOS, which further helps us to look at the atmospheric response to the described parameterizations. Section 4 describes results from sensitivity studies with using the various models. We discuss and summarize our main findings in section 5.

2 Heat flux parameterizations

The growth and decay rate $\dot{h}$ of sea ice at the ice–ocean interface is determined by the imbalance of the conductive heat flux into the ice and the oceanic heat flux F_{oce} from underneath the ice. Hence,

$$\rho_i L \dot{h}(t) = k_i \frac{\partial T}{\partial z} \mid_{ice} + F_{oce}, \tag{1}$$

where ρ_i is the density of the ice, L is the latent heat of fusion, k_i is thermal conductivity of the ice, T is temperature and z is the vertical coordinate. Some simple sea-ice models assume that sea ice has no heat capacity and does not absorb solar radiation. In these so-called zero-layer models, the temperature gradient is constant and simply given as the temperature difference between the ice surface and the ice bottom, divided by ice thickness (*Semtner*, 1976). In more advanced sea-ice models, the ice consists of several layers and the conductive heat flux into the lower most grid cell is explicitly calculated.

As discussed in the introduction, a number of approaches exist for the calculation of the oceanic heat flux F_{oce}. For the simplest, the ice-bath assumption, the temperature of the uppermost oceanic grid cell is kept at the freezing temperature. Hence, the oceanic heat flux is given as

$$F_{oce} = \frac{\rho_w c_w (T_{mix} - T_f) h_{mix}}{\delta t}, \tag{2}$$

where T_{mix} is ocean temperature, T_f is the salinity-dependent freezing temperature, ρ_w is the density of the sea water and c_w the specific heat capacity, all determined for the uppermost oceanic grid cell with vertical extent h_{mix}. δt is the time step.

In more realistic formulations, the heat flux is determined from a bulk equation based on friction velocity and temperature difference between the mixed layer and the ice–ocean interface according to

$$F_{oce} = -\rho_w c_w \alpha_h u_* (T_{mix} - T_{interface}), \tag{3}$$

where u_* is friction velocity and α_h is a turbulent heat exchange coefficient (*McPhee et al.*, 2008). A number of different formulations exist for the calculation of the interfacial temperature. Following *Schmidt et al.* (2004), these can be differentiated between a 1-equation approach, a 2-equation approach and, most realistically, a 3-equation approach. In the 1-equation approach, $T_{interface}$ is simply set to a constant value. We will not consider this approach any further here. In the more realistic 2-equation approach, $T_{interface}$ is set to the freezing temperature of the sea water in the upper-most ocean grid cell. Hence, in addition to Eq. (3), the freezing-point relationship of seawater is also required, which is the second equation of the 2-equation approach. In the most realistic 3-equation approach, $T_{interface}$ is set to the freezing temperature of the water that exists directly

https://doi.org/10.5194/gmd-2020-287
Preprint. Discussion started: 9 November 2020


Geoscientific Model Development Discussions
Open Access
EGU

at the interface. The salinity of this water is explicitly calculated from a salinity-balance equation

$$(S_{interface} - S_{ice})\dot{h}(t) = \alpha_s u_* (S_{mix} - S_{interface}). \quad (4)$$

Here, $S_{interface}$ is the salinity directly at the interface, which decreases during melting through the addition of fresher melt water of sea ice with salinity S_{ice}. Salt is exchanged with the underlying water (with salinity S_{mix}) through turbulent exchange, with a salt exchange coefficient α_S. Together with the freezing point relationship of sea water, Equations (3) and (4) form the three equations of the 3-equation approach. These three equations can be solved to calculate the three unknowns $\dot{h}$, $S_{interface}$ and $T_{interface}$.

As mentioned before, only the 3-equation approach allows for heat fluxes that are directed from the interface into the water. In addition, only the 3-equation approach allows for a realistic limitation of melt rates through the formation of a fresh water layer underneath the ice. For these reasons, significant differences can generally exist between melt rates calculated with the 3-equation approach and less realistic approaches (c.f. *Notz et al.*, 2003).

Quantitatively, a value of $0.005 < \alpha_h < 0.006$ has been found to give good agreement between measured and calculated heat fluxes for a large spread of Rayleigh numbers (*McPhee*, 2008; *McPhee et al.*, 2008). More uncertainty exists regarding the most appropriate values for the turbulent exchange coefficients α_h and α_s for the 3-equation approach. Their ratio $R = \alpha_h/\alpha_s$ depends on the molecular diffusivities for heat and salt as well as on the roughness of the boundary (*McPhee et al.*, 1987; *McPhee*, 2008). Laboratory experiments by *Owen and Thomson* (1963) and *Yaglom and Kader* (1974) imply $35 \leq R \leq 70$ (*Notz et al.*, 2003). *Sirevaag* (2009) found from an analysis of field data, $R \approx 33$, while *McPhee et al.* (2008) suggest a value of $R \approx 35$. Here we assume that the 3-equation approach with $R = 35$ best describes reality and then perform model simulations based on this approach as our reference.

During freezing conditions, salt and heat are transported almost equally efficient (*McPhee et al.*, 2008). This is because during freezing conditions, the water column is statically unstable owing to the salt release from growing sea ice. Hence, during freezing conditions, $R \approx 1$ (*McPhee et al.*, 2008), and the 2-equation approach can be used without much loss in accuracy. Best agreement with observational data is then found for $\alpha_h = 0.0057$.

In testing the impact of the various parameterizations on modeled sea ice and ocean circulation, we therefore take the following approach: for the ice-bath parameterization, we simply incorporate Eq. (2). For the 2-equation approach, we use Eq. (3) with $\alpha_h = 0.006$ and the freezing-point relationship for seawater. For the 3-equation approach, we differentiate between freezing and melting conditions. During melting, we use the full 3-equation approach with $R = 35$ as our reference. In an idealized 1-D model used in our study, $R = 70$ is also applied to test the sensitivity with respect to this parameter. For a certain value of R, we calculate α_h to satisfy the requirement described in *McPhee et al.* (1999). $R = 35$ is associated with a turbulent heat exchange coefficient of $\alpha_h = 0.0095$; and $R = 70$ with $\alpha_h = 0.0135$. During freezing, we fall back to the 2-equation approach.

https://doi.org/10.5194/gmd-2020-287
Preprint. Discussion started: 9 November 2020


Geoscientific Model Development Discussions
Open Access
EGU

3 Models

We will now briefly introduce the four different models that we use to analyse the different response to oceanic heat-flux parameterizations based on the ice-bath assumption, the 2-equation approach and the 3-equation approach. We start with a description of our idealized columnar model with simple sea ice thermodynamics, then move to the stand-alone sea ice model CICE, and finally describe the ice-ocean model MPIOM and a fully coupled model COSMOS, which consists of the oceanic component MPIOM.

3.1 Idealized 1-D model

We use a one-dimensional columnar sea-ice model coupled to a simple ocean mixed layer to carry out sensitivity studies and to investigate the impact of the three formulations for ice–ocean heat exchange in an idealised setup.

The model consists of a simple zero-layer sea-ice model, where the surface temperature T_s is determined by balancing atmospheric fluxes and the conductive heat flux through the ice according to

$$-(1-\alpha)F_{sw} - F_{other} + 0.95 \times 5.67 \times 10^{-8} {T_s}^4 = -k_i \frac{T_s - T_{bot}}{h}. \quad (5)$$

Here, α is the albedo of the ice surface, F_{sw} is the short-wave flux and F_{other} is the sum of sensible heat flux, latent heat flux and downward longwave radiation flux. $(1-\alpha)F_{sw} + F_{other}$ represents the heat input to the ocean, and $0.95 \times 5.67 \times 10^{-8} {T_s}^4$ the upward longwave radiation flux from the ocean. For simplicity, we assume that the thermal conductivity of sea ice k_i is constant and set $k_i = 2.22$ W/(m· K). During melting periods, the surface temperature is fixed at the bulk freezing temperature of the ice and the excess heat is used to melt ice at the surface. At the ice bottom, the model calculates the change in ice thickness by balancing the conductive heat flux and the oceanic heat flux according to Eq. (1).

The seasonal variation of the atmospheric fluxes F_{sw} and F_{other} are prescribed according to

$$F_{sw} = 19.5 \times exp[-0.5 \times (\frac{d - 164.1}{47.9})^2] \times 16.1$$

$$F_{other} = 117.8 \times exp[-0.5 \times (\frac{d - 206}{53.1})^2] \times 179.1,$$

where d is the number of the day in the year. Following *Notz* (2005), these two equations are a fit to the monthly-mean data compiled by *Maykut and Untersteiner* (1971). The seasonal variation in surface albedo is calculated as

$$\alpha = \frac{-0.431}{1 + (\frac{d-207}{44.5})^2} + 0.914,$$

which is a fit to measurements obtained during the SHEBA campaign (*Perovich et al.*, 1999).

The model is coupled to an idealised oceanic mixed layer of depth h_{mix}, which can store and release heat. The coupling between the mixed layer ocean and the sea ice via the oceanic heat flux F_{oce} is given by the three parameterizations as described before.

https://doi.org/10.5194/gmd-2020-287
Preprint. Discussion started: 9 November 2020


Geoscientific Model Development Discussions
Open Access
EGU

3.2 CICE

We use the stand-alone sea ice model CICE to investigate the sensitivity of sea ice to the three ice-ocean heat flux parameterizations in a modern sea-ice model. The model consists of a multi-layer energy-conserving thermodynamic sub-model (*Bitz and Lipscomb*, 1999) with a sub-grid scale ice-thickness distribution, and a submodel of ice dynamics based on an elastic-viscous-plastic rheology (*Hunke and Dukowicz*, 1997; *Hunke*, 2001) that uses incremental remapping for ice advection (*Lipscomb and Hunker*, 2004). A detailed model description is given in *Hunke and Lipscomb* (2010).

The surface temperature of the ice is calculated by balancing incoming fluxes from the atmosphere with outgoing longwave fluxes and the conductive heat flux in the ice. For the albedo, we here use the standard, so-called CCSM3 setup, where the (spectral) albedo is calculated explicitly based on snow and ice temperature and thickness (see *Hunke and Lipscomb* (2010) for details). A bulk sea ice salinity of 4 psu is implemented.

We run CICE in standalone mode, coupled to the mixed-layer ocean that forms part of the CICE package. The heat flux between this mixed-layer ocean and the sea ice is in the standard form of CICE described by the 2-equation approach with $\alpha_h = 0.006$. This formulation is here either used directly or replaced by the ice-bath formulation or the 3-equation formulation as described before. The salinity of the mixed-layer is kept at 34 g/kg.

We force CICE with the National Center for Atmospheric Research (NCAR) monthly-mean climatological data with $1^\circ \times 1^\circ$ resolution. Input fields consist of monthly climatological sea-surface temperature, sea-surface salinity, the depth of ocean mixed layer, surface wind speeds, 10 m air temperature, humidity and radiation.

3.3 MPIOM

To examine the interaction of changes in the sea-ice model with large-scale ocean circulation, we use the ocean general circulation model MPIOM (Max-Planck Institute Ocean Model). MPIOM is based on the primitive equations with representation of thermodynamic processes. A detailed description is given by *Marsland et al.* (2003).

The sea-ice component of MPIOM uses zero-layer thermodynamics following *Semtner* (1976) and viscous-plastic dynamics following *Hibler* (1979). It does not allow for a sub-grid ice-thickness distribution. The sea-ice state within a certain grid cell is hence fully described by ice concentration C and ice thickness h. The surface heat balance is solved separately for the ice covered and ice free part of every grid cell. Any ice that is formed through heat loss from the ice-free part is merged with the existing ice to form a new ice thickness and ice concentration. The distribution between thickening and a change in ice concentration is described by a distribution parameter as outlined by *Notz et al.* (2013).

In its standard setup, MPIOM uses an ice-bath parameterization to calculate the heat flux between the ocean and the ice. This formulation is either used directly or replaced by the 2-equation or the 3-equation parameterization as described before.

We run MPIOM with GR30 (about 3°) horizontal resolution and 40 uneven vertical layers, forced by daily heat, freshwater and momentum fluxes as given by the climatological OMIP forcing (*Röske*, 2006).

https://doi.org/10.5194/gmd-2020-287
Preprint. Discussion started: 9 November 2020


Geoscientific Model Development Discussions

Table 1. List of experiments

Name	Parameterization	length (model year)
SIM-icebath	Ice bath	100
SIM-2eq	2-equation	100
SIM-3eq35	3-equation, with R=35	100
SIM-3eq70	3-equation, with R=70	100
CICE-icebath	Ice bath	100
CICE-2eq	2-equation	100
CICE-3eq35	3-equation, with R=35	100
MPIOM-icebath	Ice bath	1000
MPIOM-2eq	2-equation	1000
MPIOM-3eq35	3-equation, with R=35	1000
COSMOS-icebath	Ice bath	1000
COSMOS-2eq	2-equation	1000
COSMOS-3eq35	3-equation, with R=35	1000

3.4 COSMOS

The comprehensive climate model COSMOS (ECHAM5-MPIOM), developed by the Max Planck Institute for Meteorology, is used in the present study to further investigate the atmospheric response to the three ice-ocean heat flux parameterizations. The atmosphere component ECHAM5 solves the primitive equations for the general circulation of the atmosphere on a sphere (*Roeckner et al.*, 2003). It applies Gaussian grid for horizontal transport schemes and hybrid sigma-pressure grid for the vertical between the surface and 0 hP. The OASIS3 coupler (*Valcke*, 2013) is used for the coupling between the ocean and the atmosphere components. For each day, solar and non-solar heat fluxes, hydrological variables, and horizontal wind stress are sent from the atmosphere through OASIS3 to the ocean. At the same time, the ocean transfers sea ice and sea surface temperature to the atmosphere.

The configuration of the ice-ocean component MPIOM is the same as that of the ice-ocean model MPIOM used in our study. The atmospheric module ECHAM5, was used at T31 resolution ($3.75°$) with 19 vertical levels between the surface and 0 hPa. The coupled model was initialized from a previous pre-industrial simulation and integrated with the boundary conditions, invloving the solar constant, Earth's orbital parameters and greenhouse gases, fixed at 1950 CE.

4 Results

We now turn to a description of the simulated responses of sea ice, ocean and atmosphere to the three different parameterizations. Table 1 presents the list of our experiments.

https://doi.org/10.5194/gmd-2020-287
Preprint. Discussion started: 9 November 2020


Geoscientific Model Development Discussions
Open Access
EGU

4.1 Influence of u_*, h_{mix} and the ice concentration

We start with a number of sensitivity experiments with our simple 1-D model that were carried out to understand the underlying relationship between simulated ice thickness and the three different parameterizations. We carried out four different simulations with our simple model, which in the following are called SIM-icebath, SIM-2eq, SIM-3eq35 and SIM-3eq70, where for the 3-equation setup the last number denotes the value of $R = \alpha_h/\alpha_s$, which is set to either 35 or 70. We run the simulations until the ice reaches its equilibrium thickness, with no more changes from one year to the next.

We start with examining a standard simulation with $u_* = 0.002\ m/s$, a sea-ice concentration $C = 85\%$, an albedo of sea water $\alpha_{oce} = 0.1$ and a mixed-layer depth $h_{mix} = 40$ m. The sea ice salinity is kept at 0. In winter, when the ocean loses energy to the atmosphere through the open-water part of the grid cell, the simulated heat loss from the ocean is identical in the four setups (Fig. 1c), since their open-water part is identical and the ocean is constantly at its freezing temperature (Fig. 1b). Hence, any heat that is extracted from the mixed layer directly causes ice growth, which explains the very similar accretion rates of the sea ice (Fig. 1a). Major differences between the simulations arise as soon as the net heat flux becomes positive and begins to heat the ocean. All energy that enters the ocean is then directly used to melt the ice in SIM-icebath, while some of the heat is stored in the ocean in SIM-2eq and SIM-3eq. Hence, ice in SIM-2eq and SIM-3eq melts slower than the ice in SIM-icebath, and the ocean remains warmer throughout spring (Fig. 1b). Once the ice in SIM-icebath is melted completely, the ocean temperature rises rapidly and quickly exceeds that in SIM-2eq and SIM-3eq. The slower melting of the ice in SIM-2eq and SIM-3eq and the resulting lower heat storage in the ocean throughout summer results in an earlier onset of sea-ice formation during autumn.

For SIM-icebath and SIM-2eq, the temperature at the ice-ocean interface is constant at the freezing point of the sea-water, which for our choice of $S_{seawater} = 34$ g/kg is around $-1.84\ ^\circ C$. For SIM-3eq, the interface temperature can be significantly above this value, as the interface freshens through the melting of the comparably fresh sea ice (Fig. 1d).

Comparing SIM-2eq, SIM-3eq35 and SIM-3eq70, we find that the ice thins earlier and stronger in SIM-2eq, because the ocean heat flux between the ocean and the ice is amplified in this setup owing to the constantly cold interfacial temperature. Accordingly, the oceanic temperature increases slower throughout spring in SIM-2eq. In SIM-3eq70, the transport of salt to the interface is lower than in SIM-3eq35. Hence, the interface remains fresher and warmer throughout summer. Dispite the warmer interface, stronger heat fluxes and slightly faster ablation of the ice are simulated, mainly resulting from a higher turbulent heat exchange coefficient α_h, which is 0.0095 in SIM-3eq35 and 0.0135 in SIM-3eq70.

To quantify the different response of the simulated sea-ice cover for a larger range of forcing conditions, we carried out a series of sensitivity studies. For each of these, we varied one of the forcing parameters and analysed the difference in annual mean ice thickness between SIM-3eq35 and SIM-icebath. Regarding friction velocity, we find that differences in resulting ice thickness are the larger the smaller the friction velocity is. This is related to the fact that for lower friction velocities, less heat is transported to the ice-ocean interface in the 3-equation setup, which slows down sea-ice ablation.

Regarding oceanic mixed-layer depth, we find that in our simplified setup, differences in ice thickness between SIM-3eq35 and SIM-icebath are the larger the deeper our mixed layer is. This is due to the fact that the same amount of heat input from

https://doi.org/10.5194/gmd-2020-287
Preprint. Discussion started: 9 November 2020

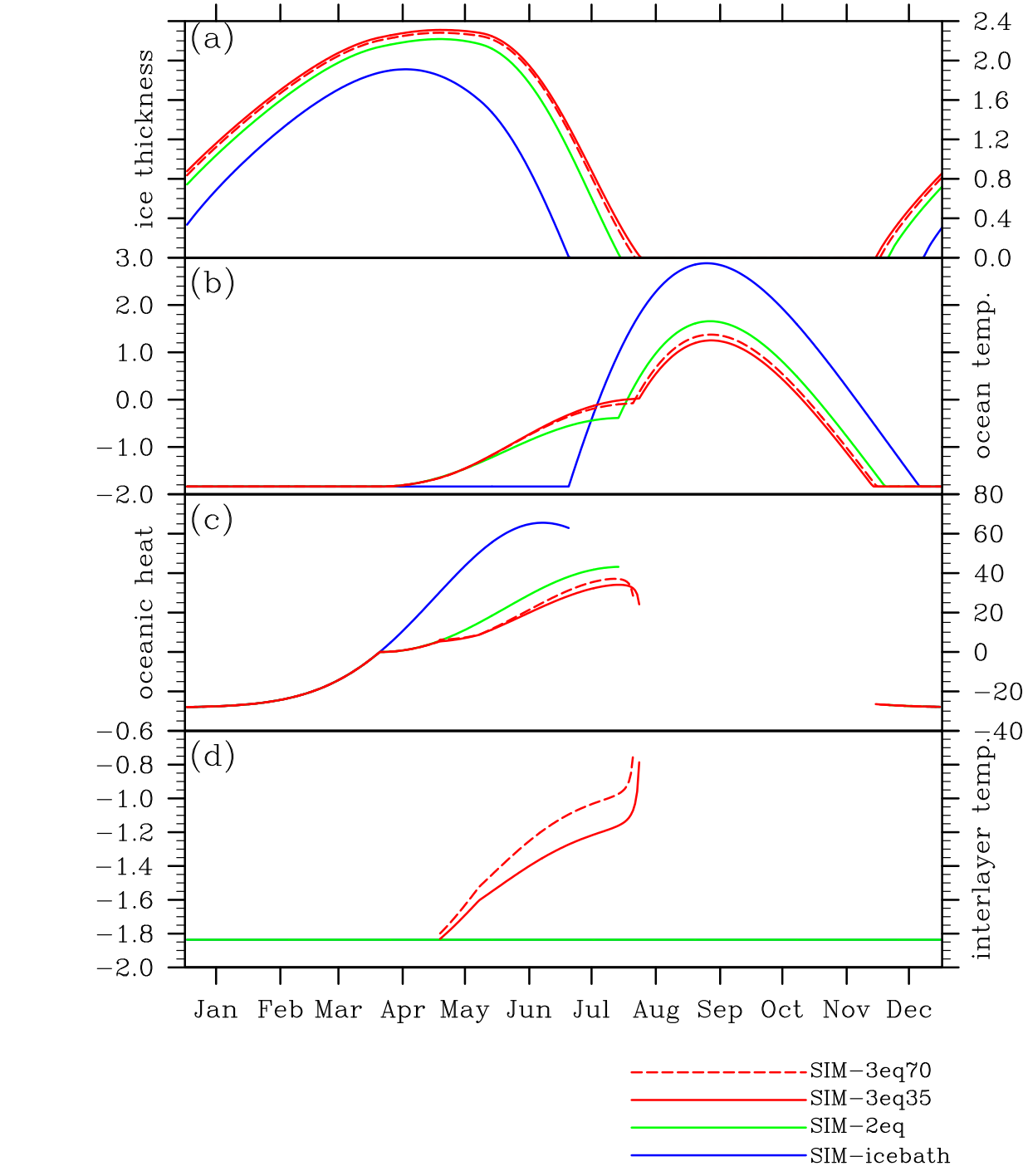

Figure 1. Time series of (a) sea-ice thickness, (b) ocean temperature, (c) ocean-to-ice heat flux and (d) ice-ocean interface temperature in the experiments SIM-icebath, SIM-2eq, SIM-3eq35 and SIM-3eq70 with friction velocity at 0.002 and ice concentration at 75%. The model is run into equilibrium.

https://doi.org/10.5194/gmd-2020-287
Preprint. Discussion started: 9 November 2020


Geoscientific Model Development Discussions

the atmosphere causes the smaller a temperature change the deeper the mixed layer is. According to equation (3), such smaller temperature change then causes a smaller heat flux to the ice bottom throughout summer. In SIM-icebath, in contrast, the ice–ocean heat flux is identical to the net flux between the air and the open water, and hence independent of the depth of the oceanic mixed layer.

Finally, regarding sea-ice concentration, we find in our simplified setup that differences in ice thickness between SIM-3eq35 and SIM-icebath are the larger the lower the ice concentration is. This is explicable by the fact that the residual energy, which mainly comes from the net incoming heat flux through open water, is all given to sea ice in SIM-icebath, while in SIM-3eq35 only a fraction of it is used for ice ablation. Lower ice concentration, namely, larger open water, amplifies the residual energy and therefore the difference in the amount of heat transferred to sea ice.

4.2 Ice thickness

Having understood some of the qualitative impact of the different parameterizations, we can now turn to an analysis of their impact in the more realistic setting provided by CICE, MPIOM and COSMOS. In these models $R = 35$ is applied in the full 3-equation approach. The presented results focus on the Arctic Ocean, as we find only minor response of the Southern Ocean properties to the change of ice-ocean heat flux parameterizations especially in MPIOM and COSMOS; furthermore, the stand-alone sea ice model CICE simulates an unrealistic distribution of sea ice in warm months in the Southern Ocean, as it fails to capture the heat release from the relatively deep mixed layer. We let all models run until the modeled ice cover (as well as the deep ocean temperatures in the cases of MPIOM and COSMOS) reaches quasi-equilibrium. In detail, we performed CICE experiments for 100 model years, with the last 10 years representing its quasi-equilibrium state. For MPIOM and COSMOS, 1000-model-year experiments were conducted, and data from the last 100 model years were used for analysis. Significance level was calculated by performing Student's t-test which considers the interannual variances of the last 100 simulation years (10 years in the case of CICE). Doing so, we find a similar response in ice thickness to the different parameterizations as in the simple, one-dimensional model: Everything else unchanged, the ice-bath parameterization leads compared to the 3-equation approach to thinner ice throughout the Arctic Ocean, both in winter and summer (Fig. 2). The change is similar but less pronounced in the simulations based on the 2-equation parameterization. The most significant changes occur in the marginal ice zone where sea-ice concentration is lowest, again consistent with the results from the one-dimensional model. In the Arctic, the change in March thickness is generally less pronounced than the change in September thickness. This is due to the fact that the air-to-ocean heat flux tends to be negative (the ocean loses heat to the air) in March, and both the temperature of the water and the temperature at the ice-ocean interface are maintained at the freezing point. Hence, in all parameterizations, the extracted heat is directly transfered into sea-ice formation. In September, in contrast, the ocean can maintain a temperature above the freezing temperature in the 2-equation or 3-equation approach but not in the ice-bath approach. Hence, as in the simple 1-D model, differences between the different parameterizations are more pronounced during summer. In addition, sea-ice concentration is high throughout March, which reduces the direct interaction of atmospheric heat fluxes with the ocean. As discussed in the previous subsection, this limits differences between the different parameterizations during winter time. Finally, the ice thins somewhat less in winter because of dynamical effects: the thinner ice is more mobile and more prone to ridging,

https://doi.org/10.5194/gmd-2020-287
Preprint. Discussion started: 9 November 2020

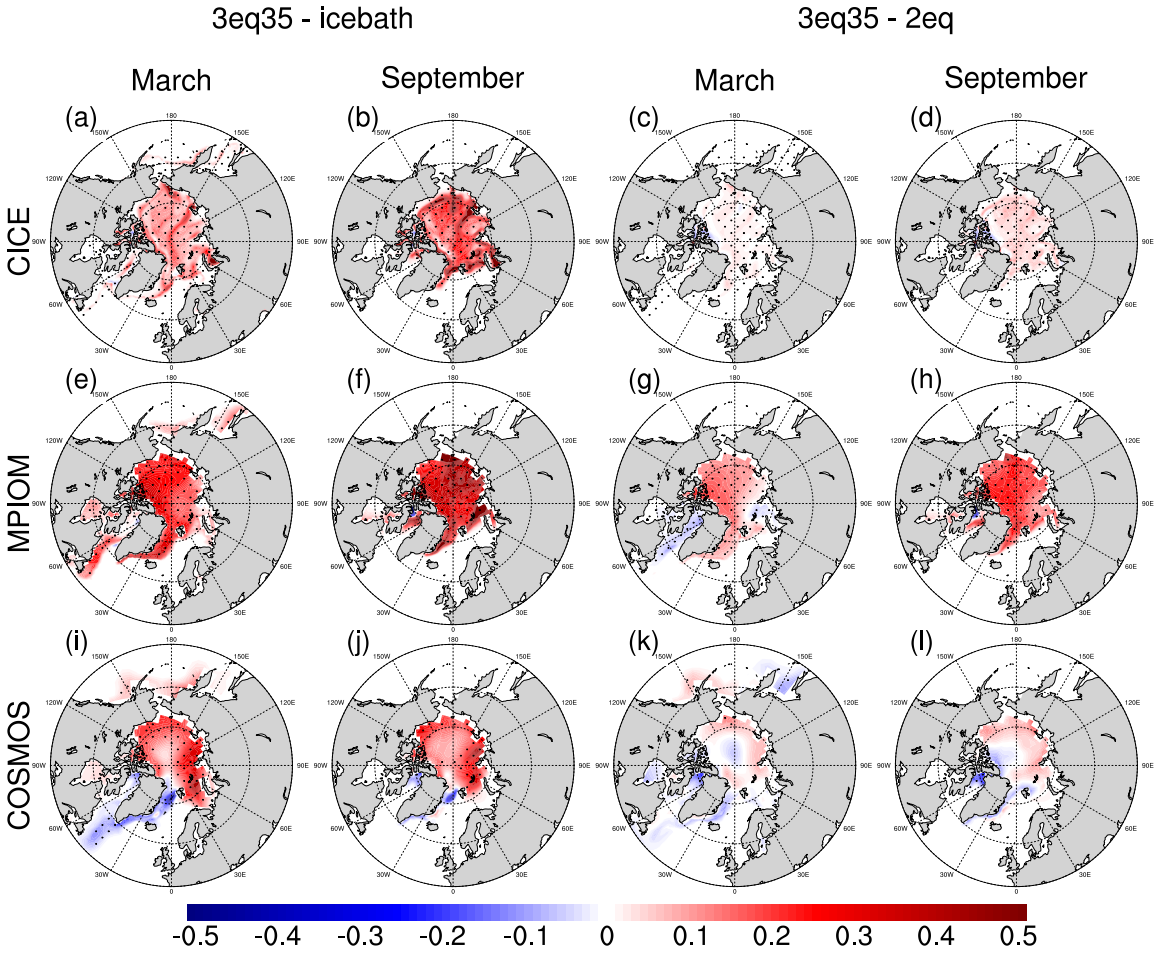

Figure 2. The difference in the Arctic sea-ice thickness for (a) CICE-3eq35 – CICE-icebath in March, (b) CICE-3eq35 – CICE-icebath in September, (c) CICE-3eq35 – CICE-2eq in March, (d) CICE-3eq35 – CICE-2eq in September, (e) MPIOM-3eq35 – MPIOM-icebath in March, (f) MPIOM-3eq35 – MPIOM-icebath in September, (g) MPIOM-3eq35 – MPIOM-2eq in March, (h) MPIOM-3eq35 – MPIOM-2eq in September, (i) COSMOS-3eq35 – COSMOS-icebath in March, (j) COSMOS-3eq35 – COSMOS-icebath in September, (k) COSMOS-3eq35 – COSMOS-2eq in March, and (l) COSMOS-3eq35 – COSMOS-2eq in September. The marked area has a significance level of greater than 95% based on Student's t-test. Units: m.

https://doi.org/10.5194/gmd-2020-287
Preprint. Discussion started: 9 November 2020

Geoscientific Model Development Discussions
Open Access
EGU

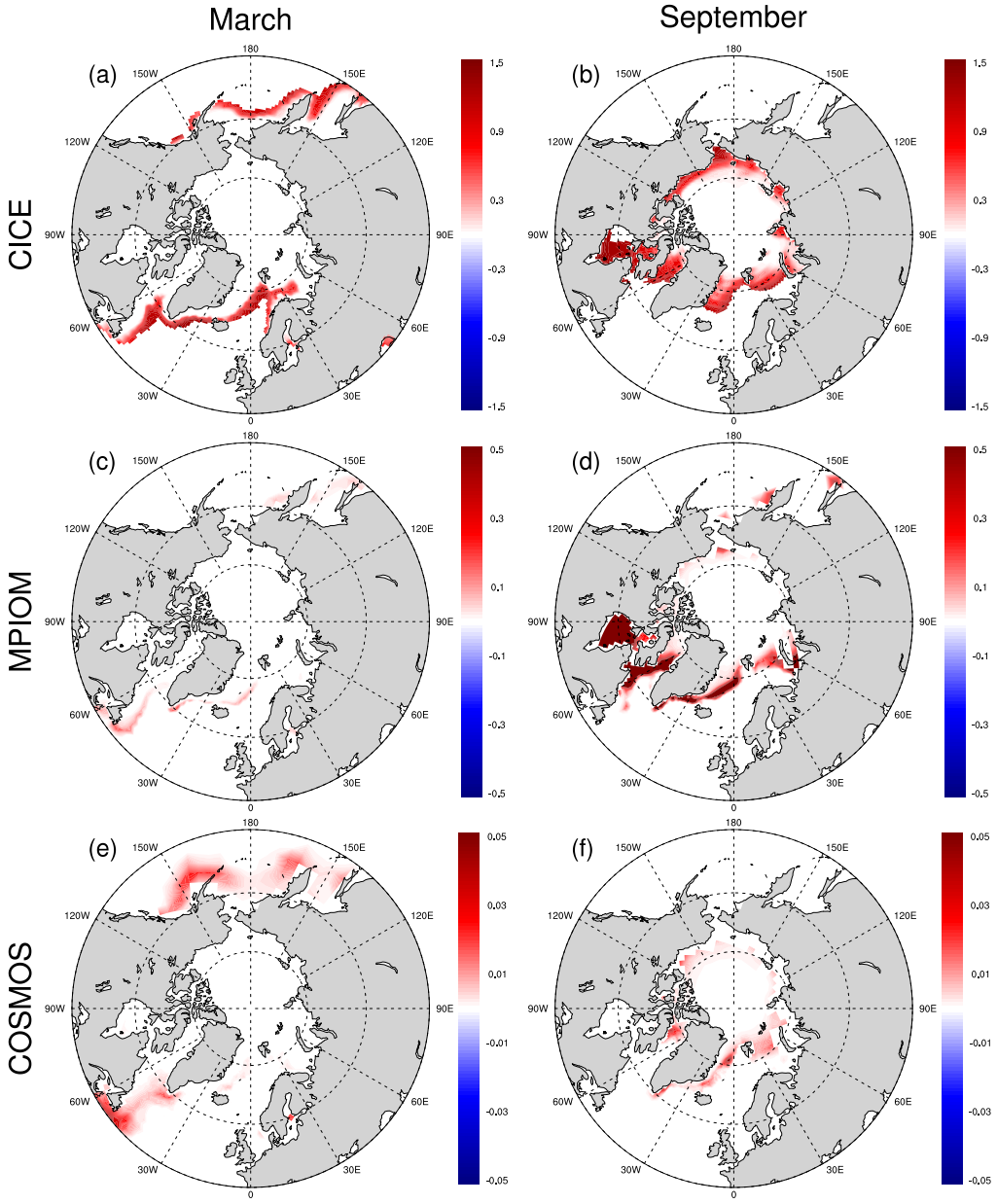

Figure 3. The anomaly of the Arctic ice-ocean interface temperature in (a-b) CICE-3eq35, (c-d) MPIOM-3eq35, and (e-f) COSMOS-3eq35 relative to freezing point of the far-field ocean (about -1.8°). The left column is for March and the right column for September. Units: K.

https://doi.org/10.5194/gmd-2020-287
Preprint. Discussion started: 9 November 2020


Geoscientific Model Development Discussions

255 which fosters the formation of areas with open water. In these areas, significant amounts of new ice can form, which dampens some of the thermodynamic thinning of the ice pack. Among the three parameterizations, only the 3-equation approach can obtain a temperature above the freezing point of the far-field ocean at the the interface between the ice and the salt water (Fig. 3), which can slow down the ocean-to-ice heat flux. This is due to the fact that the ice-ocean interface is usually very fresh owing to the ablation of the ice bottom. When the temperature of the interface exceeds that of the mixed layer, a reversed heat 260 flux from the ice to the ocean can occur.

4.3 Upper ocean temperature and salinity

We now move on to analyse how the described changes in sea ice impact upper ocean temperature and salinity. We find for the Arctic Ocean that the ice-bath parameterization and the 2-equation approach result in almost the same temperature distribution during winter as the more realistic 3-equation approach in CICE and MPIOM (Fig. 4a,c,e,g). During summer, however, the ice- 265 bath approach causes warmer water to persist around the ice edge in CICE (Fig. 4b). This is caused by the fact that here the ice melts earlier than in the 3-equation approach, which then allows the ocean to absorb heat more efficiently. The same is found in MPIOM in the areas of Hudson Bay, Baffin-Bay and Norwegian Sea and Barents Sea (Fig. 4f,h). The most intriguing feature found in COSMOS is a significant cooling across the North Atlantic Ocean in the ice-bath and 2-equation parameterizations compared to the 3-equation approach (Fig. 4i-l). Such cooling is a consequence of weakened thermohaline circulation which 270 tends to bring relatively warmer water from the lower latitudes (illustrated in Section 4.4).

Because brine is released from sea-ice during its formation and growth, the changes in ice thickness between different parameterizations should trigger changes in upper ocean salinity. Indeed, we find such changes to occur (Fig. 5): In regions in which the ice-bath approach or the 2-equation approach cause an increased heat flux to the ice underside, and hence a reduction in ice thickness, the ocean is generally less salty in these simulations with a simplified parameterization of ice–ocean 275 heat exchange than in the simulations with the full 3-equation parameterization. Interestingly, the opposite sign is observed in coastal regions of the Arctic Ocean in COSMOS-icebath, both in winter and summer (Fig. 5e-f), despite the larger melt rates of the simplified scheme. This is explicable by the fact that less ice mass is accumulated at the coastal areas in the experiment with ice-bath parameterization, thus less brine can be released during ice ablation period. The North Atlantic Ocean experiences a pronounced freshening in the ice-bath approach in COSMOS (Fig. 5e-f), which lowers the efficiency of deep-water formation. 280 No significant change in upper ocean salinity is revealed between experiments COSMOS-2eq and COSMOS-3eq35 (Fig. 5g-h).

4.4 Thermohaline structure of the ocean

We now turn to the large-scale changes in the thermohaline structure of the ocean. We find that compared to the more realistic 3-equation approach, the ice-bath and 2-equation approaches lead to significant cooling of the ocean's deep water masses (Fig. 6c,e,g). This behaviour is due to the fact that the heat flux out of the ocean is slowed down in the 3-equation approach, 285 therefore more heat can be stored in the mixed layer and further advects to deep ocean. However, the opposite sign is observed in experiment MPIOM-icebath, which results in a pronounced warming in the deep water masses by up to 0.5 °C (Fig. 6a).

https://doi.org/10.5194/gmd-2020-287
Preprint. Discussion started: 9 November 2020

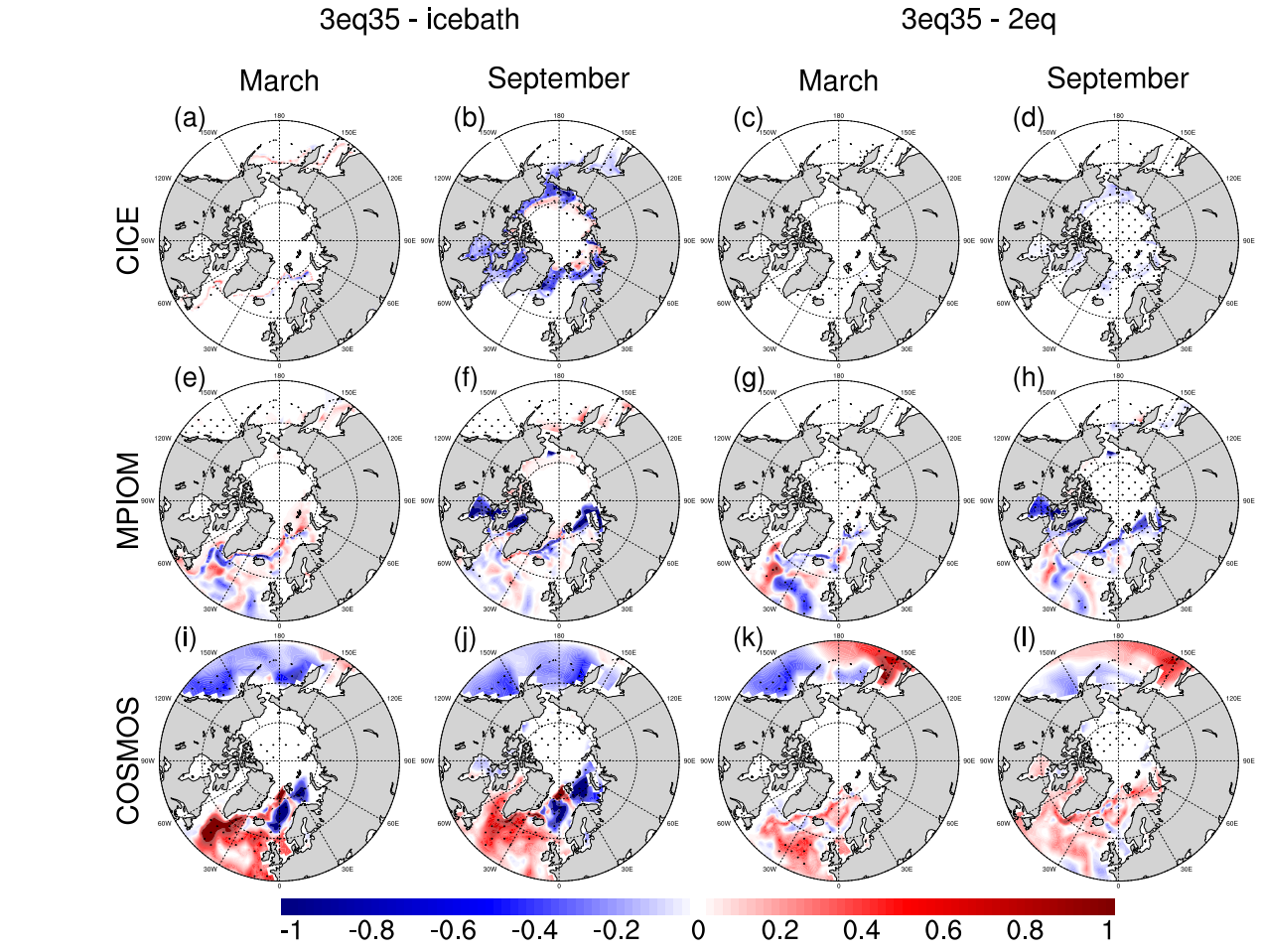

Figure 4. As in Fig. 2, but for the sea surface temperature. Units: K.

https://doi.org/10.5194/gmd-2020-287
Preprint. Discussion started: 9 November 2020

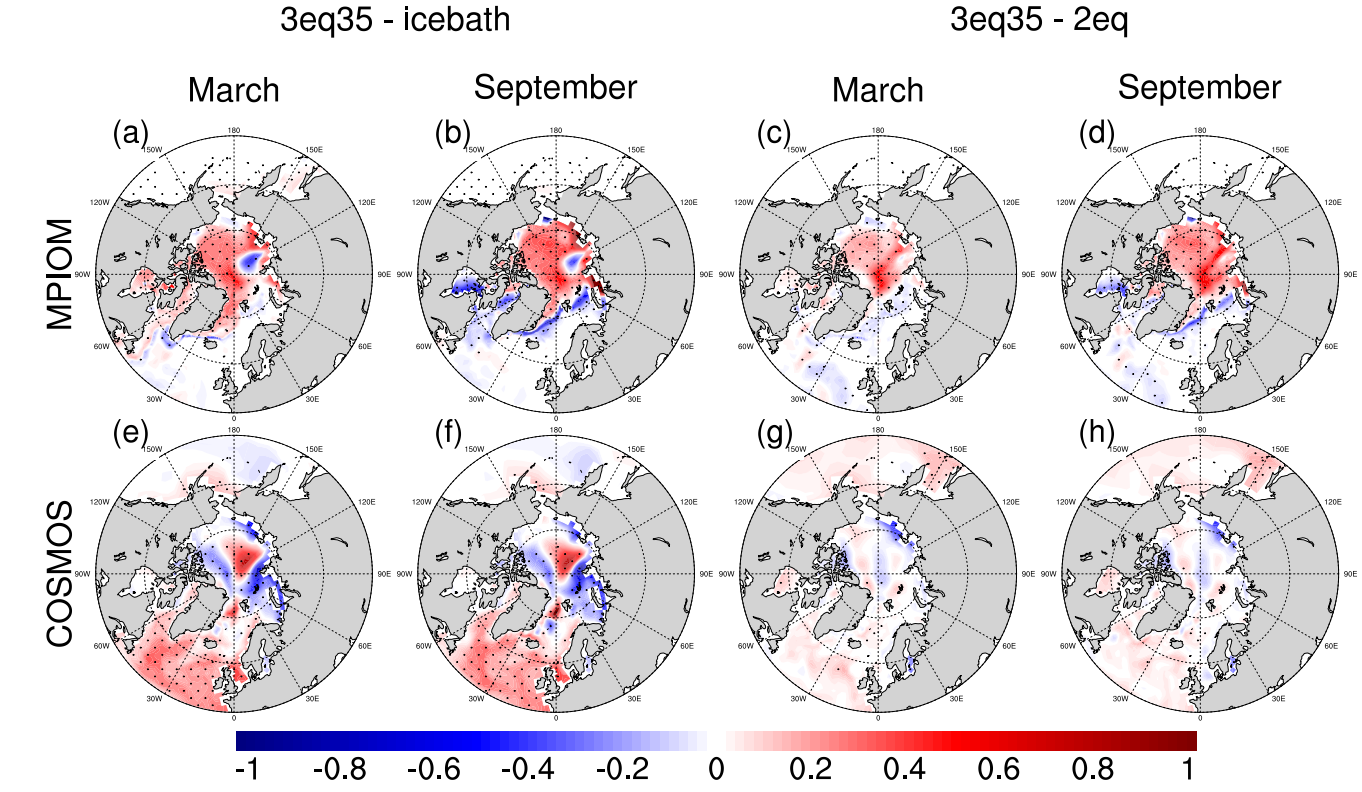

Figure 5. As in Fig. 2e-l, but for the sea surface salinity. Units: g/kg.

https://doi.org/10.5194/gmd-2020-287
Preprint. Discussion started: 9 November 2020

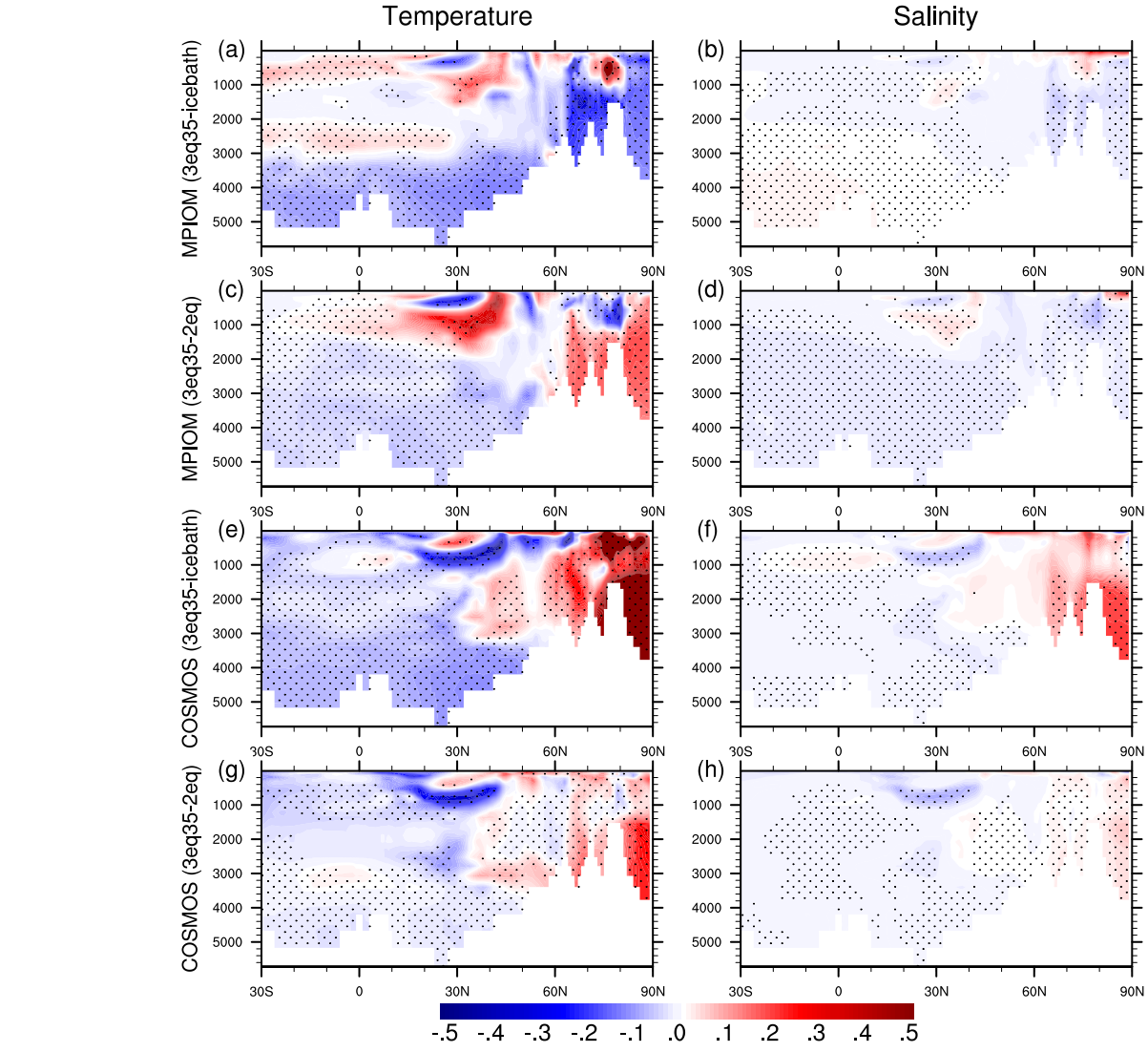

Figure 6. Anomalies in temperature and salinity vertical profile across the North Atlantic section (-80-0°W) (a,b) MPIOM-3eq35 – MPIOM-icebath, (c,d) MPI-3eq35 – MPI-2eq, (e,f) COSMOS-3eq35 – COSMOS-icebath, and (g,h) COSMOS-3eq35 – COSMOS-2eq. The left column is for temperature and the right column for salinity. Units: K and g/kg.

https://doi.org/10.5194/gmd-2020-287
Preprint. Discussion started: 9 November 2020


Geoscientific Model Development Discussions

Table 2. AMOC index

Experiment	AMOC index	NP index
MPIOM-icebath	20.1	-
MPIOM-2eq	20.2	-
MPIOM-3eq35	20.2	-
COSMOS-icebath	16.6	1017.5
COSMOS-2eq	16.8	1017.4
COSMOS-3eq35	17.6	1017.9

This warming in the simulations with the least realistic parameterization of ice–ocean heat exchange reflects its earlier ice loss in areas of deep-water formation, which causes enhanced surface warming of the water there.

As the simplified parameterizations both lead to thinner sea ice throughout the Arctic Ocean compared to the most realistic approach, one would expect a freshening of the ocean mixed layer and the deep water mass that originates from such fresher surface source water. Indeed, we find that such freshening in MPIOM occurs only within the Arctic upper ocean between depths of 0 and 100 m (Fig. 6b,d). In COSMOS, the freshening extends to the bottom of the Arctic Ocean (Fig. 6f,h). Such different model behaviour is currently not understood.

The Atlantic meridional overturning circulation (AMOC) streamfunction — defined as the zonally integrated transport over the Atlantic basin, shows a weakening over 40-60°N, 0-3000 m depth in MPIOM-icebath and MPIOM-2eq compared to MPIOM-3eq35. In COSMOS, a pronounced weakening of AMOC is obtained south of 60°N. The AMOC index, i.e. the maximum value of AMOC streamfunction over the region of 800-2000 m depth, 20-90°N is found to be 20.2 Sv and 17.6 Sv ($1Sv = 10^6 m^3/s$) in MPIOM-3eq35 and COSMOS-3eq35, respectively (Table 2). The latter is consistent with the estimates of global circulation from hydrographic data (15±3 Sv) (*Ganachaud and Wunsch*, 2000). Compared to the corresponding 3-equation approach, the strength of the AMOC decreases by 1 Sv and 0.8 Sv in COSMOS-icebath and COSMOS-2eq respectively (Table 2). In COSMOS-icebath, the reduced sea surface salinity in the Atlantic section (Fig. 5e-f, Fig. 6f) lowers the efficiency of deep-water formation, resulting in a weakening of the AMOC (Fig. 7c). A similar but less pronounced pattern is obtained by COSMOS-2eq (Fig. 6h). No significant anomaly in the AMOC index is found in MPIOM (Table 2).

4.5 Atmosphere responses

We now finally turn to investigate how the sea ice changes affect the atmospheric properties in the fully coupled model COSMOS.

The response in surface air temperature, as shown in Fig. 8, indicates a general warming over the Arctic Ocean and its adjacent continents in the COSMOS-icebath and COSMOS-2eq compared to COSMOS-3eq35; while the opposite sign can be found for the Greenland, Nordic Sea, North Atlantic Ocean, southeastern North America, and mid-latitude Eurasia. There are various reasons responsible for these changes: 1) Reduced Arctic sea ice mass in the ice-bath and 2-equation approaches lead to a decrease in the surface albedo, resulting in more heat flux absorbed by the surface. 2) The decline of AMOC in experiments

https://doi.org/10.5194/gmd-2020-287
Preprint. Discussion started: 9 November 2020

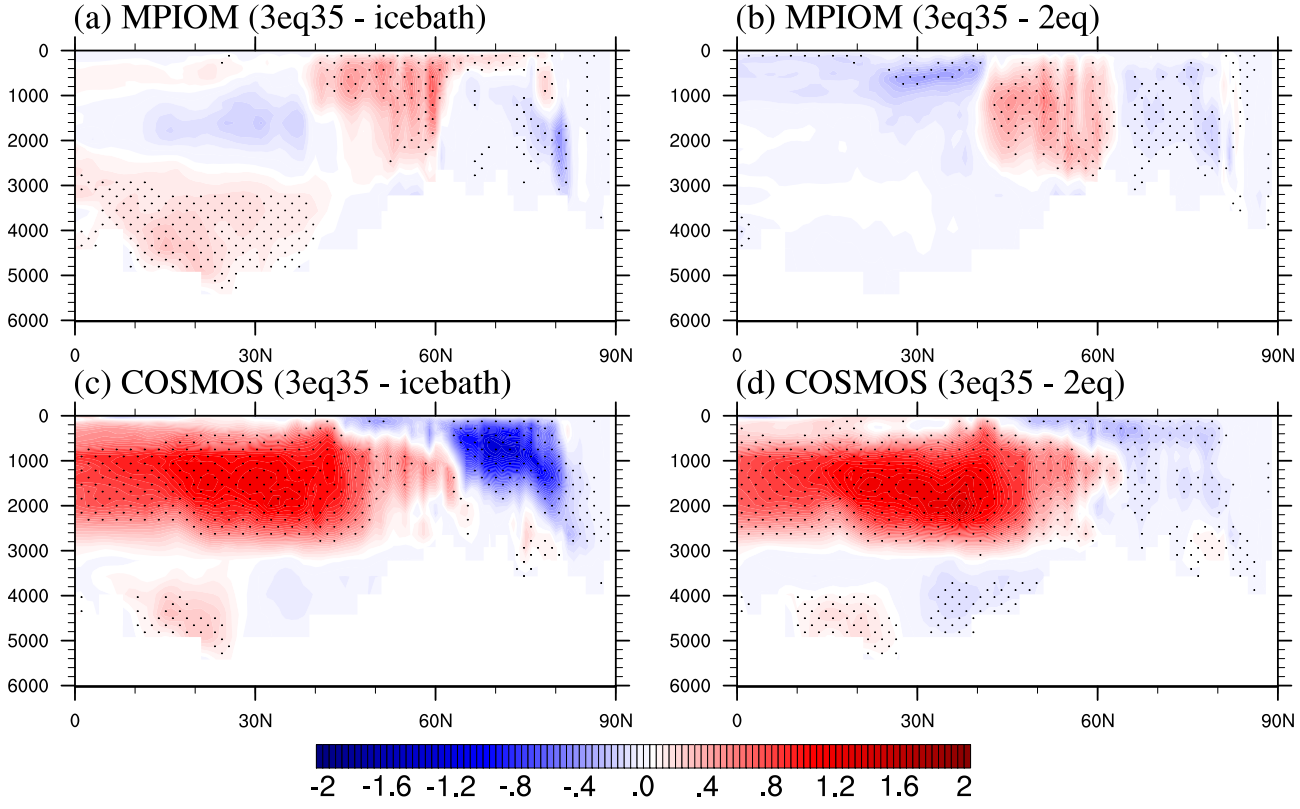

Figure 7. Anomalies in AMOC (a) MPIOM-3eq35 – MPIOM-icebath, (b) MPI-3eq35 – MPI-2eq, (c) COSMOS-3eq35 – COSMOS-icebath, and (d) COSMOS-3eq35 – COSMOS-2eq. Units: Sv.

https://doi.org/10.5194/gmd-2020-287
Preprint. Discussion started: 9 November 2020

Geoscientific Model Development
Discussions
Open Access
EGU

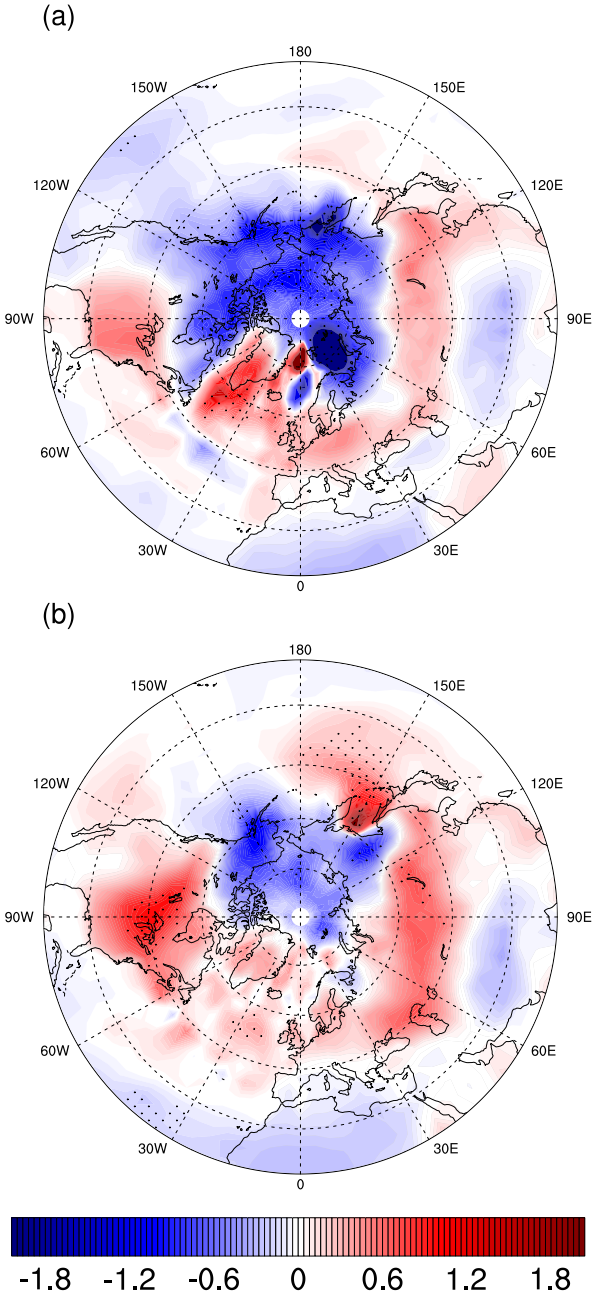

Figure 8. Anomalies in surface air temperature (a) COSMOS-3eq35 – COSMOS-icebath, and (b) COSMOS-3eq35 – COSMOS-2eq. Units: K.

https://doi.org/10.5194/gmd-2020-287
Preprint. Discussion started: 9 November 2020


Geoscientific Model Development Discussions

COSMOS-icebath and COSMOS-2eq weakens the northward heat transport from lower latitudes to North Atlantic regions. 3) The atmospheric circulation also plays a role, which is discussed in the following.

Fig. 9 depicts the responses in boreal winter sea level pressure (SLP). Compared to the most realistic parameterization, the simplified approaches illustrate a more negative North Atlantic Oscillation (NAO) mode, with positive SLP anomalies over the Greenland and Nordic seas and negative anomalies over the North Atlantic subtropical zone. SLP anomalies in another time window show similar pattern (Fig. S1), indicating the robustness of the NAO- signal in the simplified approaches, even though the significance level does not exceed 95%. Composite analysis shows that a positive NAO mode leads to a warming over much of Europe and far downstream as winter-time enhanced westerly flow across the North Atlantic moves relatively warm and moist maritime air to that region (Fig. S2a). Another notable feature is the cooling and warming over North Africa and North America respectively, which is associated with the stronger clockwise flow around the subtropical Atlantic high-pressure center. These described patterns are consistent with the modeled surface air temperature response over Northern Hemisphere continents (Fig. 8).

The anomalous NAO pattern can also lead to significant changes in the ocean circulation. The convective activities in the Labrador Sea and the Greenland-Iceland-Norwegian (GIN) Seas are shown to have important contributions to the production and transport of North Atlantic deep water (Fig. S3a), and therefore drive the North Atlantic thermohaline circulation. We find that the intensity of the the Labrador Sea convection is characterized by variations that appear to be synchronized with variabilities in the NAO (Fig. S3b). Therefore, the weakening of AMOC in our simplified setups compared to the most realistic approach can be attributed to the simulated anomalous negative NAO phase.

Another intriguing pattern in the atmosphere is an anomalous negative SLP over the North Pacific Ocean in the simplified parameterizations compared to the most realistic approach. Here we calculate the North Pacific (NP) index as the area-weighted SLP over the region of 30-65°N, 160°E-140°W during boreal winter (*Trenberth and Hurrell*, 1994). The NP index in COSMOS-3eq35 is shown to be 0.4-0.5 hPa higher than its counterparts (Table 2). A high NP index leads to a warming over southern North America and the northern Eurasia, as well as a cooling over northern North America (Fig. S2b), resembling the pattern of the surface air temperature anomalies (Fig. 8). Therefore, the response of the surface air temperature in the simplized parameterizations can be attributed to the combined effect of the weakened AMOC and NAO, and the enhanced Aleutian Low.

5 Discussion and conclusion

In the present study, we perform 1-D simulations with an idealized columnar model (SIM), as well as global simulations with a stand-alone sea ice model (CICE), an ice-ocean coupled model (MPIOM), and a fully coupled climate model COSMOS, to analyze the sensitivity of modeled climate to ice-ocean interface heat flux parameterizations. This is achieved by implementing into the models: 1) a simple ice-bath assumption with the ocean temperature fixed at the freezing temperature, 2) a more realistic bulk 2-equation with freezing temperature kept at the ice–ocean interface and the ocean being allowed to be warmer than freezing point (*McPhee*, 1992) and 3) a most advanced double diffusional transport (3-equation) approach with the temperature at the ice–ocean interface being calculated based on the melting rate of the ice bottom (*Notz et al.*, 2003).

https://doi.org/10.5194/gmd-2020-287
Preprint. Discussion started: 9 November 2020

Geoscientific Model Development Discussions
Open Access
EGU

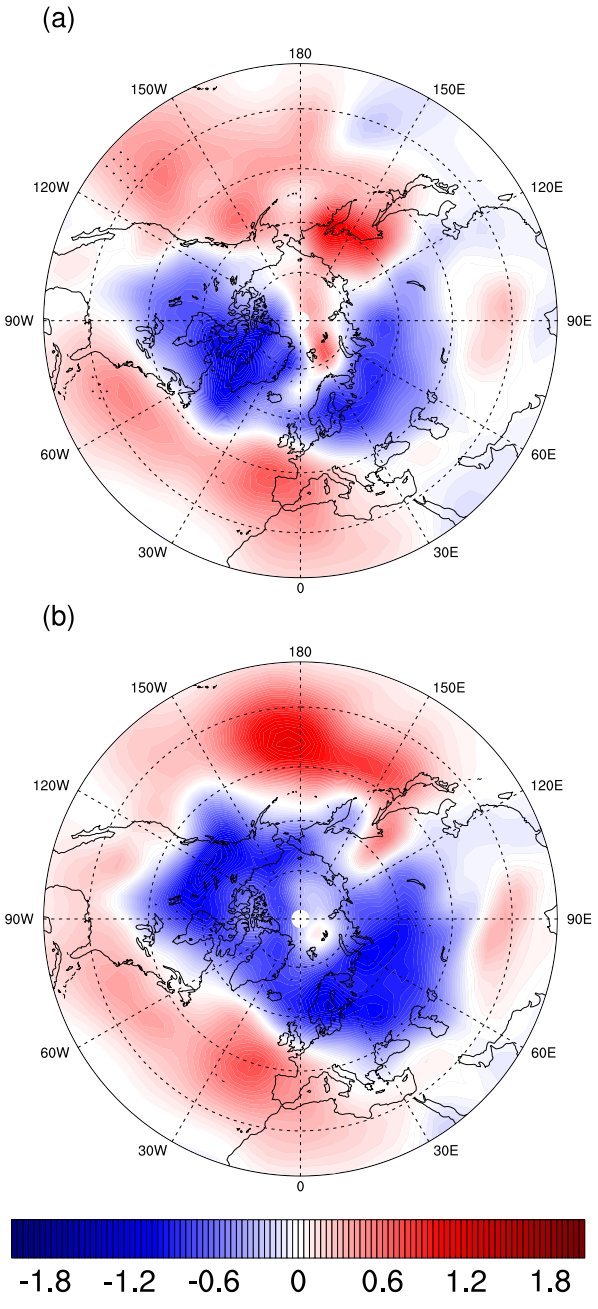

Figure 9. Anomalies in boreal winter sea level pressure (a) COSMOS-3eq35 – COSMOS-icebath, and (b) COSMOS-3eq35 – COSMOS-2eq. Units: hPa.

https://doi.org/10.5194/gmd-2020-287
Preprint. Discussion started: 9 November 2020

The conclusions drawn from these models in terms of sea ice properties are quite similar with each other: The thinnest ice is observed in the ice-bath simulations, as no residual heat is allowed to remain in water, therefore the sea water beneath sea ice is constantly at its freezing point. The 2-equation experiments simulate a relatively thicker sea ice, because some of the heat is stored in the ocean rather than used for ice growth. The simulated sea ice by the 3-equation approach has the largest thickness, as the temperature at the ice-ocean interface can exceed the freezing point of the far-field ocean, thus the heat flux out of the ocean can be slowed or even reversed. The ice marginal areas are found to be highly sensitive to the choice of ice-ocean heat flux parameterizations. Furthermore, the sea water temperature in the ice marginal zones is largely determined by the onset/retreat of the sea ice.

As a result of the brine release during sea ice formation, the Arctic Ocean is most and least salty in the 3-equation experiment and the ice-bath experiment respectively; the same is found in the deep water masses due to their coupling with the surface source water. The thermohaline instability obtained from such salinity profile is responsible for a strengthening of the Atlantic meridional overturning circulation (AMOC) in the coupled simulation with the 3-equation approach.

COSMOS reveals intensification in both AMOC and NAO when the most advanced ice-ocean heat flux parameterization is applied. It has long been recognized that the NAO variability has an important influence on deep convection in the North Atlantic subpolar regions (*Curry et al.*, 1998). Ocean observations and model simulations show that the changes in the thermohaline circulation during the last century have been driven by low-frequency variations in the NAO via changes in Labrador Sea convection (*Latif et al.*, 2006). More recently, a delayed oscillator model as well as a climate model suggest that the NAO forces the AMOC on a 60-year cycle (*Sun et al.*, 2015). The strengthening in AMOC, obtained in our COSMOS-3eq experiment, is likely due to the combined effect of increased thermohaline instability and the amomalous NAO+ mode. In contrast, no obvious response of AMOC can be found in the MPIOM experiments (Table 2). This is due to the fact that MPIOM uses prescribed atmospheric forcings which largely limits the air-sea interaction feedback.

Our study indicates a less pronounced sea-ice response to ice-ocean interface heat flux parameterizations in the fully coupled climate model COSMOS than in the ice-ocean model MPIOM (compare Fig. 2e-h with Fig. 2i-l). This is because the change of AMOC has a damping effect on the simulated sea ice anomalies. The strengthening of AMOC in COSMOS-3eq can lead to a warming over the Northern Hemisphere, especially over the North Atlantic and the Arctic. This hypothesized link between AMOC and Northern Hemisphere mean surface climate has been documented in an abundance of studies (e.g., *Schlesinger and Ramankutty*, 1994; *Rühlemann et al.*, 2004; *Dima and Lohmann*, 2007; *Parker et al.*, 2007). The AMOC-induced warming helps to reduce the sea ice mass over the Arctic and North Atlantic subpolar regions. Indeed, the sea ice across the Greenland Sea and Baffin Bay are found to be thinnest in COSMOS-3eq.

In the present paper, we exclude the responses of the Southern Ocean, as they are found to be much less pronounced than those of the Arctic Ocean. Another reason lies on the over-estimation of the Southern Ocean sea ice extent by the stand-alone sea ice model CICE due to a lack of represented warm deep water.

The presented study gives us a better understanding of the importance of a realistic representation of ice-ocean heat flux processes in large scale-climate models, including their effect on sea ice, ocean circulation, and the atmosphere. We find that

https://doi.org/10.5194/gmd-2020-287
Preprint. Discussion started: 9 November 2020


Geoscientific Model Development Discussions

substantial, large scale climate metrics can emerge from the different parameterization, highlighting the importance of a careful evaluation of their impact in climate-model simulations.

Code and data availability. The source code, data as well as scripts for plotting the figures in this manuscript can be downloaded from "https://gitlab.awi.de/xshi/ice-ocean-heat-flux". A snapshot of this repository has been submitted to Zenodo with a granted doi number of 10.5281/zenodo.4160368.

Author contributions. D. Notz, J. Liu and X. Shi developed the original idea for this study. X. Shi and H. Yang contribute to the code modification and model simulation under the supervision of J. Liu (for CICE), D. Notz (for SIM and MPIOM), and G. Lohmann (for COSMOS). All authors contribute to the data analysis, discussion and paper writing.

Competing interests. The authors have declared that no competing interests exist.

https://doi.org/10.5194/gmd-2020-287
Preprint. Discussion started: 9 November 2020

Acknowledgements. This research is supported by the National Key R&D Program of China (2018YFA0605901) and NSFC (41676185); the Institute of Atmospheric Physics, Chinese Academy of Sciences (IAP/CAS); Max Planck Institute for Meteorology (MPI-M); Alfred Wegener Institute, Helmholtz center for Polar and Marine Research; PACMEDY of the Belmont Forum; the second phase of PALMOD project, and the open fund of State Key Laboratory of Loess and Quaternary Geology, Institute of Earth Environment, CAS (SKLLQG1920). D. Notz is funded by the Deutsche Forschungsgemeinschaft under Germany's Excellence Strategy EXC 2037 'CLICCS - Climate, Climatic Change, and Society' Project Number: 390683824, contribution to the Center for Earth System Research and Sustainability (CEN) of Hamburg University. In addition, we would like to thank Karl-Hermann Wieners, Helmuth Haak, Xiucheng Wang and Mirong Song for their technical help with the MPIOM and CICE models, and thank Nils Fischer for very interesting discussions.

https://doi.org/10.5194/gmd-2020-287
Preprint. Discussion started: 9 November 2020

Geoscientific Model Development Discussions

References

Bitz, C. M., and W. H. Lipscomb (1999), An enery–conserving thermodynamic model of sea ice, *J. Geophys. Res.*, *104*(C7), 15,669–15,677.

Curry, R. G., M. S. McCartney, and T. M. Joyce (1998), Oceanic transport of subpolar climate signals to mid-depth subtropical waters, *Nature*, *391*(6667), 575–577.

Dima, M., and G. Lohmann (2007), A hemispheric mechanism for the atlantic multidecadal oscillation, *J. Clim.*, *20*(11), 2706–2719.

Ganachaud, A., and C. Wunsch (2000), Improved estimates of global ocean circulation, heat transport and mixing from hydrographic data, *Nature*, *408*(6811), 453–457.

Hibler, W. D. (1979), A dynamic thermodynamic sea ice model, *J. Phys. Oceanogr.*, *9*(4), 815–846.

Hunke, E. C. (2001), Vicous–plastic sea ice dynamics with the EVP model: Linearization issues, *J. Comput. Phys.*, *170*, 18–39.

Hunke, E. C., and J. K. Dukowicz (1997), An Elastic–Viscous–Plastic model for sea ice dynamics, *J. Phys. Oceanogr.*, *27*, 1849–1867.

Hunke, E. C., and W. H. Lipscomb (2010), CICE documentation and user's guide.

Jenkins, A., H. H. Hellmer, and D. M. Holland (2001), The role of meltwater advection in the formulation of conservative boundary conditions at an ice–ocean interface, *J. Phys. Oceanogr.*, *31*, 285–296.

Josberger, E. G. (1983), Sea ice melting in the marginal ice zone, *J. Geophys. Res.*, *88*(C5), 2841–2844.

Latif, M., C. Böning, J. Willebrand, A. Biastoch, J. Dengg, N. Keenlyside, U. Schweckendiek, and G. Madec (2006), Is the thermohaline circulation changing?, *Journal of Climate*, *19*(18), 4631–4637.

Lipscomb, W. H., and E. C. Hunker (2004), Modeling sea ice transport using incremental remapping, *Mon. Wea. Rev.*, *132*, 1341–1354.

Marsland, S., H. Haak, J. Jungclaus, M. Latif, and F. Röske (2003), The Max-Planck-Institute global ocean/sea ice model with orthogonal curvilinear coordinates, *Ocean Model.*, *5*(2), 91–127, https://doi.org/10.1016/S1463-5003(02)00015-X.

Maykut, G. A., and N. Untersteiner (1971), Some results from a Time-dependent thermodynamic Model of sea ice, *J. Geophys. Res.*, *76*(6), 1550–1575.

McPhee, M. (2008), *Air-Ice-Ocean Interaction: Turbulent Ocean Boundary Layer Exchange Processes*, Springer Verlag.

McPhee, M., J. H. Morison, and F. Nilsen (2008), Revisiting heat and salt exchange at the ice-ocean interface: Ocean flux and modeling considerations, *J. Geophys. Res.*, *113*(C6), C06,014.

McPhee, M. G. (1986), The upper ocean, *The Geophysics of Sea Ice*, pp. 339–394.

McPhee, M. G. (1992), Turbulent heat flux in the upper ocean under sea ice, *J. Geophys. Res.*, *97*(C4), 5365–5379.

McPhee, M. G., G. A. Maykut, and J. H. Morison (1987), Dynamics and thermodynamics of the ice/upper ocean system in the marginal ice zone of the Greenland sea, *J. Geophys. Res.*, *92*(C7), 7017–7031.

McPhee, M. G., C. Kottmeier, and J. H. Morison (1999), Ocean heat flux in the central weddell sea during winter, *Journal of Physical Oceanography*, *29*(6), 1166–1179.

Mellor, G. L., M. G. McPhee, and M. Steele (1986), Ice-seawater turbulent boundary layer interaction with melting or freezing, *J. Phys. Oceanogr.*, *16*, 1829–1846.

Notz, D. (2005), Thermodynamic and fluid-dynamical processes in sea ice, *Univ. of Cambridge*, Ph.D. thesis.

Notz, D., M. G. McPhee, M. G. Worster, G. A. Maykut, K. H. Schlünzen, and H. Eicken (2003), Impact of underwater-ice evolution on Arctic summer sea ice, *Journal of Geophysical Research: Oceans*, (C7).

Notz, D., F. A. Haumann, H. Haak, J. H. Jungclaus, and J. Marotzke (2013), Arctic sea-ice evolution as modeled by Max Planck Institute for Meteorology's Earth system model, *Journal of Advances in Modeling Earth Systems*, *5*(2), 173–194.

https://doi.org/10.5194/gmd-2020-287
Preprint. Discussion started: 9 November 2020

Owen, P. R., and W. R. Thomson (1963), Heat transfer across rough surfaces, *J. Fluid Mech.*, *15*, 321–334.

Parker, D., C. Folland, A. Scaife, J. Knight, A. Colman, P. Baines, and B. Dong (2007), Decadal to multidecadal variability and the climate change background, *Journal of Geophysical Research: Atmospheres*, *112*(D18).

Perovich, D. K., and G. A. Maykut (1990), Solar heating of a stratified ocean in the presence of a static ice cover, *J. Geophys. Res.*, *95*(C10), 18,233–18,245.

Perovich, D. K., T. C. Grenfell, B. Light, J. A. RichterMenge, M. Sturm, W. V. Tucker III, H. Eicken, G. A. Maykut, and B. Elder (1999), SHEBA: Snow and Ice Studies CD-ROM, *Tech. rep.*, Cold Regions Research and Engineering Laboratory.

Roeckner, E., et al. (2003), The atmospheric general circulation model ECHAM5: Part 1: Model description, Deutsches Klimarechenzentrum, 349, 1–140.

Røed, L. P. (1984), A thermodynamic coupled ice-ocean model of the marginal ice zone, *J. Phys. Oceanogr.*, *14*, 1921–1929.

Röske, F. (2006), A global heat and freshwater forcing dataset for ocean models, *Ocean Modelling*, *11*, 235–297.

Rühlemann, C., S. Mulitza, G. Lohmann, A. Paul, M. Prange, and G. Wefer (2004), Intermediate depth warming in the tropical atlantic related to weakened thermohaline circulation: Combining paleoclimate and modeling data for the last deglaciation, *Paleoceanography*, *19*(PA1025), PA1025, https://doi.org/10.1029/2003PA000948.

Schlesinger, M. E., and N. Ramankutty (1994), An oscillation in the global climate system of period 65-70 years, *Nature*, (367), 723–726.

Schmidt, G., C. Bitz, U. Mikolajewicz, and L. Tremblay (2004), Ice-ocean boundary conditions for coupled models, *Ocean Model.*, *7*(1-2), 59–74.

Semtner, A. J. (1976), A model for the thermodynamic growth of sea ice in numerical investigations of climate, *J. Phys. Oceanogr.*, *6*(3), 379–389.

Sirevaag, A. (2009), Turbulent exchange coefficients for the ice/ocean interface in case of rapid melting, *Geophys. Res. Lett.*, *36*(4), L04,606.

Sun, C., J. Li, and F.-F. Jin (2015), A delayed oscillator model for the quasi-periodic multidecadal variability of the NAO, *Climate Dynamics*, *45*(7-8), 2083–2099.

Trenberth, K. E., and J. W. Hurrell (1994), Decadal atmosphere-ocean variations in the Pacific, *Climate Dynamics*, *9*(6), 303–319.

Valcke, S. (2013), The OASIS3 coupler: a European climate modelling community software, *Geoscientific Model Development*, *6*(2), 373–388.

Yaglom, A. M., and B. A. Kader (1974), Heat and mass transfer between a rough wall and turbulent fluid flow at high Reynolds and Peclet numbers, *J. Fluid Mech.*, *62*, 601–623.